Journal of GeoEngineering, Vol. 15, No. 3, pp. 159-171, September 2020
http://dx.doi.org/10.6310/jog.202009_15(3).5

EXACT STIFFNESS METHOD FOR MULTI-LAYERED SATURATED SOILS UNDER MOVING DYNAMIC LOADS

Teerapong Senjuntichai [1*], Suraparb Keawsawasvong [2], and Bundid Yooyao [3]

ABSTRACT

In this paper, dynamic response of multi-layered poroelastic soils subjected to moving loads is presented by adopting an exact stiffness matrix method. The soil medium under consideration consists of a number of layers overlying a homogeneous half-space. The exact stiffness matrices for each layer and the half-space are obtained explicitly from the analytical general solution derived by applying the triple-dimensional Fourier transformation to the governing equations based on Biot's poroelastodynamics theory. The solution to the global equation system yields displacements and pore pressure in the Fourier transform domain at the layer interfaces. Time domain solutions are obtained by applying the fast Fourier transform (FFT) and an accurate numerical quadrature scheme. Comparison with existing solutions on moving load problems is presented to verify the accuracy of the present solution scheme. A parametric study is then carried out to investigate the influence of various parameters on displacements and pore pressure of multi-layered saturated soils under moving loads. The proposed solution scheme is also extended to study dynamic interaction between flexible pavement under a moving load and multi-layered soils.

Key words: Exact stiffness matrix method, flexible pavement, moving loads, multi-layered saturated soils, poroelasticity.

1. INTRODUCTION

The study of dynamic response of supporting soils under moving vehicle loads is of considerable importance in the field of geotechnical engineering due to its close relevance to various practical problems. For example, the analysis of ground vibrations induced by surface and underground high-speed trains and a subway system has useful applications in the design of railways, pavement and tunnels. In the past, several researchers have investigated various moving load problems related to single-phase elastic soils (*e.g.,* Sneddon 1952; Eason 1965; Keer 1969; Barros and Luco 1994; Jones *et al.* 1997; Grundmann *et al.* 1999; Hung and Yang 2001; Lefeuve-Mesgouez *et al.* 2002; Si *et al.* 2016; Ai and Ren 2016; Ai *et al.* 2018). Geo-materials often consist of solid skeletons with pore spaces filled with water, commonly known as poroelastic materials, which are widely considered to be better representation of natural soils and rocks than single-phase elastic materials. The theory of wave propagations in poroelastic materials was presented by Biot (Biot 1956, 1962), who added the inertia terms to his quasi-static theory (Biot 1941). Biot's poroelastodynamics theory has been widely employed to study a variety of geotechnical problems related to poroelastic soils (*e.g.,* Zeng and Rajapakse 1999; Senjuntichai and Kaewjuea 2008; Kaewjuea *et al.* 2014; Ai and Wang 2017; Hu *et al.* 2017; Senjuntichai *et al.* 2018).

For moving load problems on saturated soils, Burke and Kingsbury (1984) investigated a homogeneous poroelastic medium subjected to moving surface traction with a constant velocity. A semi-analytical method was employed by Siddharthan *et al.* (1993) to present dynamic response of a saturated soil layer under a moving surface line load. Dynamic response of a poroelastic half-plane was also reported by Theodorakopoulos (2003) and Jin *et al.* (2004). The steady state response of a poroelastic half space under a moving rectangular load case was studied by Cai *et al.* (2007), who later examined dynamic response of a track–ground system due to a moving train by employing a substructure technique (Cai *et al.* 2008). In addition, problems of a homogeneous poroelastic half-space under a moving truck and a high-speed train were also presented by Cai *et al.* (2015) and Liu *et al.* (2017), respectively. The studies mentioned above are concerned with various types of moving loading on homogeneous saturated soil media. A review of literature indicates that studies related to multi-layered soils under moving loads are very limited when compared with homogeneous cases despite the fact that natural soil profiles are horizontally layered with different properties and thicknesses. In the past, dynamic response of multi-layered poroelastic soils was investigated by employing two main approaches, namely, the transmission and reflection matrix (TRM) approach and the stiffness matrix approach. The conventional TRM approach is known to have numerical instability due to the presence of mismatching exponential terms appearing in the layer matrices. Improved formulations were later developed based on the TRM approach by several researchers to study dynamic response of layered media including multi-layered poroelastic half-space subjected to moving loads (Xu *et al.* 2008; Lefeuve-Mesgouez and Mesgouez 2012).

This paper presents dynamic response of multi-layered saturated soils subjected to moving loads as shown in Fig. 1 by adopting an exact stiffness matrix method. In this approach, the stiffness matrices that describe the relationship between generalized

Manuscript received January 23, 2020; revised July 6, 2020; accepted July 12, 2020.
[1*] Professor (corresponding author), Applied Mechanics and Structures Research Unit, Department of Civil Engineering, Faculty of Engineering, Chulalongkorn University, Bangkok, Thailand (e-mail: Teerapong.S@chula.ac.th).
[2] Lecturer, Department of Civil Engineering, Thammasat School of Engineering, Thammasat University, Pathumthani, Thailand.
[3] Former Graduate Student, Applied Mechanics and Structures Research Unit, Department of Civil Engineering, Faculty of Engineering, Chulalongkorn University, Bangkok, Thailand.

displacement and force vectors of each layer and the underlying half-space are derived explicitly from the general solutions in the Fourier transform space, which are obtained analytically from Biot's poroelastodynamics equations (Biot 1962). The global stiffness matrix and the global force vector of the multi-layered system are assembled by considering the continuity of traction and fluid discharge at each layer interface. The displacements and pore pressure in the multi-layered soils under moving dynamic loads can then be determined by solving the global stiffness equation for discrete values of horizontal wave numbers and frequency. Time domain solutions can finally be obtained by employing the fast Fourier transform (FFT) and an accurate numerical quadrature. The accuracy of the developed solution scheme is verified by comparing with existing solutions of moving load problems related to elastic and poroelastic soils. Selected numerical results are presented to demonstrate the influence of various parameters such as loading speed and poroelastic material parameters on displacements and pore pressure in multi-layered soils subjected to moving loads. In addition, the applicability of the present stiffness matrix scheme to geotechnical problems is also demonstrated by investigating a dynamic soil-structure interaction problem between flexible pavement under a moving load and a multi-layered saturated soil medium.

2. PROBLEM FORMULATION

2.1 Problem Description

Consider a multi-layered poroelastic soil medium defined with a Cartesian coordinate subjected to a moving load as shown in Fig. 1. Each layer and an underlying half-space of the soil medium are perfectly bonded and governed by Biot's poroelastodynamics theory (Biot 1962). In addition, the load is moving with constant velocity and vertically applied to the free surface of the soil medium. For the analysis of pavement-soil interaction as shown in Fig. 2, the pavement is modeled as an infinite elastic plate, which behaves according to the Kirchhoff small deflection thin plate theory. In addition, the contact between the pavement and the soil medium is assumed to be smooth and either permeable or impermeable.

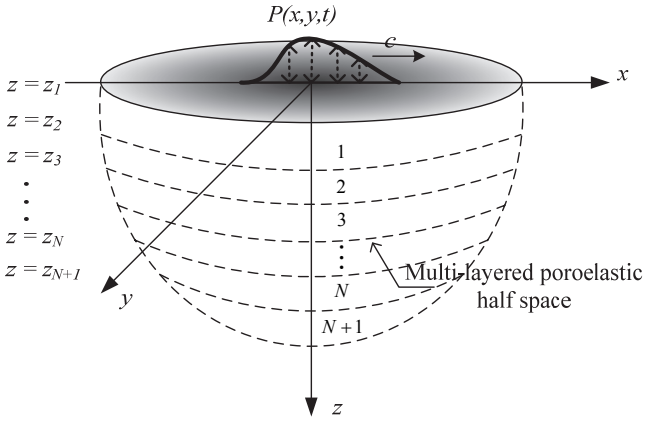

Fig. 1 Multi-layered poroelastic soils under moving dynamic load

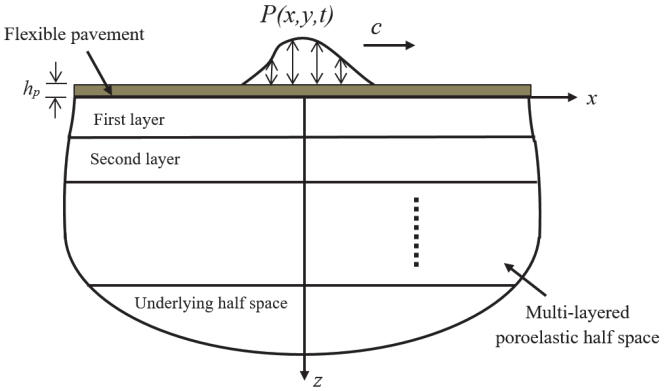

Fig. 2 Flexible pavement on multi-layered poroelastic soils under moving dynamic load

2.2 Basic Equations and General Solutions

Let u_i ($i = x, y, z$) and w_i ($i = x, y, z$) denote the average displacement of the solid matrix and the fluid displacement relative to the solid matrix in the i-direction ($i = x, y, z$), respectively. The constitutive relations of a poroelastic material (Biot 1941), can be expressed as;

$$\sigma_{ij} = 2\mu\varepsilon_{ij} + \lambda\delta_{ij}\varepsilon_{kk} - \alpha\delta_{ij}p, \quad i, j = x, y, z \tag{1a}$$

$$p = -M(\alpha\varepsilon_{kk} + w_{i,i}) \tag{1b}$$

where σ_{ij} is the total stress component; ε_{ij} is the strain component; μ and λ denote Lame' constants; δ_{ij} is the Kronecker delta; p denotes the excess pore fluid pressure where suction is considered negative; and α and M are Biot's parameters accounting for compressibility of the poroelastic medium. For all poroelastic materials, $0 \le \alpha \le 1$ and $0 < M < \infty$. For a completely dry material, $M \to 0$ whereas $\alpha \le 1$ and $M \to \infty$ for a material with incompressible constituents. In addition, the fluid discharge in the i-direction, denoted by q_i, can be defined in term of the fluid displacement w_i as $q_i = \partial w_i/\partial t$. Note that air bubbles and fluid are considered together as part of the constituents of pororelastic materials.

The equations of motions for a poroelastic material, in the absence of body forces and a fluid source, can be written in the standard indicial notation as (Biot 1962):

$$\mu u_{i,jj} + (\lambda + \alpha^2 M + \mu)u_{i,ji} + \alpha M w_{j,ji} = \rho\ddot{u}_i + \rho_f\ddot{w}_i \tag{2a}$$

$$\alpha M u_{j,ji} + M w_{j,ji} = \rho_f\ddot{u}_i + m\ddot{w}_i + b\dot{w}_i \tag{2b}$$

In Eq. (2), the superscript dot denotes the derivative with respect to the time variable; ρ and ρ_f are the mass densities of the bulk material and the pore fluid, respectively; and m is a density-like parameter that depends on ρ_f and the pore geometry. In addition, b is a parameter accounting for the internal friction due to the relative motion between solid matrix and pore fluid. The parameter b is equal to the ratio between the fluid viscosity and the intrinsic permeability of the medium. If internal friction is neglected, $b = 0$. It should be noted that the equations of motions, Eqs. (2a) and (2b), do not have six independent unknowns of u_i and w_i ($i = x, y, z$). With the aid of Eq. (1b), Eqs. (2) can be reduced to four independent equations expressed in terms of the four basic unknowns, *i.e.,* u_x, u_y, u_z, and p.

The triple-Fourier integral transform, and its inverse relationship can be written, respectively as:

$$\overline{f}(k_x, k_y, z, \omega) = \int_{-\infty}^{\infty}\int_{-\infty}^{\infty}\int_{-\infty}^{\infty} f(x, y, z, t)\, e^{-ik_x x - ik_y y - i\omega t}\, dx\, dy\, dt \tag{3a}$$

$$f(x, y, z, t) = \frac{1}{(2\pi)^3}\int_{-\infty}^{\infty}\int_{-\infty}^{\infty}\int_{-\infty}^{\infty} \overline{f}(k_x, k_y, z, \omega)\, e^{ik_x x + ik_y y + i\omega t}\, dk_x\, dk_y\, d\omega \tag{3b}$$

where k_x and k_y are the wave numbers associated with the x and y coordinates, respectively. In addition, ω is the frequency of motion, and i is the unit imaginary number.

It can be shown that the general solutions of the displacements and the pore pressure can be obtained in the Fourier transform domain as (Lu and Jeng 2007):

$$\overline{u}_x = -\mathrm{i}k_x(a_1 Ae^{-\gamma_1 z} + a_1 Be^{\gamma_1 z} + a_2 Ce^{-\gamma_2 z} + a_2 De^{\gamma_2 z}) - \frac{\mathrm{i}\gamma_3}{k_x}(Ee^{-\gamma_3 z} - Fe^{\gamma_3 z}) - \frac{\mathrm{i}k_y}{k_x}(Ge^{-\gamma_3 z} + He^{\gamma_3 z}) \tag{4a}$$

$$\overline{u}_y = -\mathrm{i}k_y(a_1 Ae^{-\gamma_1 z} + a_1 Be^{\gamma_1 z} + a_2 Ce^{-\gamma_2 z} + a_2 De^{\gamma_2 z}) + \mathrm{i}Ge^{-\gamma_3 z} + \mathrm{i}He^{\gamma_3 z} \tag{4b}$$

$$\overline{u}_z = a_1\gamma_1(Ae^{-\gamma_1 z} - Be^{\gamma_1 z}) + a_2\gamma_2(Ce^{-\gamma_2 z} - De^{\gamma_2 z}) + Ee^{-\gamma_3 z} + Fe^{\gamma_3 z} \tag{4c}$$

$$\overline{p} = Ae^{-\gamma_1 z} + Be^{\gamma_1 z} + Ce^{-\gamma_2 z} + De^{\gamma_2 z} \tag{4d}$$

where the superposed bar denotes the triple-Fourier transforms of a function, and A, B, …, to H are the arbitrary functions to be determined by applying appropriate boundary and continuity conditions. In addition,

$$a_i = \frac{\lambda\chi_i + \mu\chi_i - \alpha + \left[\rho_f\omega^2/(m\omega^2 - \mathrm{i}b\omega)\right]}{\mu(S^2 - L_i^2)},\quad i = 1, 2 \tag{5a}$$

$$\gamma_i^2 = k_x^2 + k_y^2 - L_i^2,\ i = 1, 2\ ;\quad \gamma_3^2 = k_x^2 + k_y^2 - S^2 \tag{5b}$$

$$L_1^2 = \frac{\beta_1 + \sqrt{\beta_1^2 - 4\beta_2}}{2};\quad L_2^2 = \frac{\beta_1 - \sqrt{\beta_1^2 - 4\beta_2}}{2} \tag{5c}$$

$$S^2 = \frac{\omega^2\left\{\rho - \left[\rho_f^2\omega^2/(m\omega^2 - \mathrm{i}b\omega)\right]\right\}}{\mu} \tag{5d}$$

$$\beta_1 = \frac{(m\omega^2 - \mathrm{i}b\omega)(\lambda + \alpha^2 M + 2\mu) + \rho M\omega^2 - 2\alpha M\rho_f\omega^2}{M(\lambda + 2\mu)};$$

$$\beta_2 = \frac{(m\omega^2 - \mathrm{i}b\omega)\rho\omega^2 - \rho_f^2\omega^4}{M(\lambda + 2\mu)} \tag{5e}$$

$$\chi_i = \frac{\vartheta M L_i^2 - \rho_f\omega^2}{\rho_f M\omega^2(\alpha - \vartheta)},\quad i = 1, 2 \tag{5f}$$

The general solutions for stresses and fluid displacements can be obtained from the general solutions given in Eq. (4), and the constitutive relations, Eq. (1), and they are given elsewhere (Lu and Jeng 2007). In addition, ϑ is defined in Eq. (A.44).

2.3 Moving Load Function

According to Hung and Yang (2001), the function of moving load $P(x, y, t)$ as shown in Fig. 1 can be represented by:

$$P(x, y, t) = P_o\,\phi(x - ct)\,\delta(y)\,f(t) \tag{6}$$

where P_o denotes the magnitude of moving load; $\phi(x - ct)$ is the distribution function, which is related to the distribution of the applied load passing a fixed point; c is the velocity of moving load; and $f(t)$ is the dynamic function represents the dynamic interaction between the loading and the soil medium. In addition, $\delta(\ )$ denotes a Dirac delta function, which has the following property:

$$\int_a^c f(x)\,\delta(x - b)dx = f(b);\qquad a < b < c \tag{7}$$

The application of the triple-Fourier transform to Eq. (6), together with the above property of the Dirac delta function yields:

$$\overline{P}(k_x, k_y, \omega) = P_o\,\tilde{\phi}(k_x)\,\tilde{f}(\omega + k_x c) \tag{8}$$

where $\tilde{\phi}(k_x)$ and $\tilde{f}(\omega + k_x c)$ denote the one-dimensional Fourier transforms of $\phi(x)$ and $f(t)$ respectively. In this study, it is assumed that $f(t)$ only depends on a single frequency ω_0, which can be expressed as:

$$f(t) = \mathrm{e}^{i\omega_0 t} \tag{9}$$

For the above dynamic function $f(t)$, $\tilde{f}(\omega + k_x c)$ is then given by:

$$\tilde{f}(\omega + k_x c) = \frac{1}{c}\delta\left(\frac{\omega - \omega_0}{c} + k_x\right) \tag{10}$$

where $\delta(\ )$ is a Dirac delta function. It is noted that if $\omega_0 = 0$ then $f(t) = 1$, and the case of a moving load with no oscillation is considered. For the case with non-zero ω_0, a moving load is oscillating at a constant frequencies of $f_0 = \omega_0/(2\pi)$.

3. EXACT STIFFNESS MATRICES

In this paper, an exact stiffness matrix method is employed to investigate the dynamic response of multi-layered saturated soils to moving loads. A brief outline of the exact stiffness matrix scheme is presented here, and more details on the application of this method for three-dimensional dynamic response of multi-layered poroelastic media can be found in Senjuntichai *et al.* (2019). Figure 1 shows a multi-layered half-space consisting of N poroelastic layers with different properties and thicknesses overlying a homogenous poroelastic half-space subjected to a moving load $P(x, y, t)$. Let a superscript n denotes the quantities related to the nth soil layer (n = 1, 2, 3, …, N). The following matrices can be defined for the nth layer:

$$\mathbf{u}^{(n)}=\begin{bmatrix}\left\{i\bar{u}_x^{(n)}(k_x,k_y,z_n) \quad i\bar{u}_y^{(n)}(k_x,k_y,z_n) \quad \bar{u}_z^{(n)}(k_x,k_y,z_n) \quad \bar{p}^{(n)}(k_x,k_y,z_n)\right\}^T \\ \cdots\cdots \\ \left\{i\bar{u}_x^{(n)}(k_x,k_y,z_{n+1}) \quad i\bar{u}_y^{(n)}(k_x,k_y,z_{n+1}) \quad \bar{u}_z^{(n)}(k_x,k_y,z_{n+1}) \quad \bar{p}^{(n)}(k_x,k_y,z_{n+1})\right\}^T\end{bmatrix} \tag{11}$$

$$\boldsymbol{\sigma}^{(n)}=\begin{bmatrix}\left\{-\bar{\sigma}_{xz}^{(n)}(k_x,k_y,z_n) \quad -\bar{\sigma}_{yz}^{(n)}(k_x,k_y,z_n) \quad -\bar{\sigma}_{zz}^{(n)}(k_x,k_y,z_n) \quad -\bar{w}_z^{(n)}(k_x,k_y,z_n)\right\}^T \\ \cdots\cdots \\ \left\{\bar{\sigma}_{xz}^{(n)}(k_x,k_y,z_{n+1}) \quad \bar{\sigma}_{yz}^{(n)}(k_x,k_y,z_{n+1}) \quad \bar{\sigma}_{zz}^{(n)}(k_x,k_y,z_{n+1}) \quad \bar{w}_z^{(n)}(k_x,k_y,z_{n+1})\right\}^T\end{bmatrix} \tag{12}$$

In Eq. (11), $\mathbf{u}^{(n)}$ denotes a generalized displacement vector whose elements are the Fourier transforms of displacements and pore pressure, which are the four basic unknowns, at the top and bottom surfaces of the nth layer. In addition, $\boldsymbol{\sigma}^{(n)}$, given by Eq. (12), denotes a generalized force vector whose elements are the Fourier transforms of stresses and fluid displacement, which are employed in the representation of traction and fluid source, respectively, at the top and bottom surfaces of the nth layer. The following relationship can then be established for the nth layer:

$$\boldsymbol{\sigma}^{(n)}=\mathbf{K}^{(n)}\mathbf{u}^{(n)}, \quad n=1, 2, 3, \cdots, N \tag{13}$$

where $\mathbf{K}^{(n)}$ is defined as an exact stiffness matrix in the frequency-wave number domain describing the relationship between the generalized displacement and force vectors $\mathbf{u}^{(n)}$ and $\boldsymbol{\sigma}^{(n)}$, respectively for the nth soil layer. Similarly, the stiffness matrix for the underlying half-space $\mathbf{K}^{(n+1)}$ can be obtained from the relationship between the generalized displacement and force vectors, $\mathbf{u}^{(N+1)}$ and $\boldsymbol{\sigma}^{(N+1)}$, for the underlying half-space. The elements of the stiffness matrices $\mathbf{K}^{(n)}$ and $\mathbf{K}^{(n+1)}$ are given explicitly in the Appendix.

Finally, the following global stiffness equation is established by enforcing the continuity of traction and fluid flow at all layer interfaces:

$$\mathbf{K_G}\,\mathbf{U_G}=\mathbf{F_G} \tag{14}$$

where $\mathbf{K_G}$ is the global stiffness matrix; $\mathbf{U_G}$ is the global vector of generalized displacements; and $\mathbf{F_G}$ is the global vector of generalized forces defined as:

$$\mathbf{F_G}=[\mathbf{T}^{(1)}\ \mathbf{T}^{(2)} \ldots\ \mathbf{T}^{(N+1)}]^{\mathrm{T}} \tag{15a}$$

in which,

$$\mathbf{T}^{(k)}=\left[\ \bar{T}_x^{(k)} \quad \bar{T}_y^{(k)} \quad \bar{T}_z^{(k)} \quad \frac{\bar{T}_q^{(k)}}{i\omega}\ \right]^{\mathrm{T}} \quad (k=1, 2, 3, \ldots, N+1) \tag{15b}$$

In addition, $\bar{T}_i^{(k)}$ and $\bar{T}_q^{(k)}$ denote the triple-Fourier transform of traction in the i-direction ($i = x, y, z$) and fluid discharge, respectively, which are applied at the kth layer interface (k = 1, 2, 3, …, N + 1).

For the boundary value problem shown in Fig. 1, the elements in $\mathbf{T}^{(k)}$ (k = 1, 2, 3,…, N + 1) are all zero except that $\bar{T}_z^{(1)}=-\bar{P}(k_x,k_y,\omega)$, which is the triple-Fourier transform of the moving load $P(x, y, t)$. For a fully permeable top surface of multi-layered saturated soils, $\bar{p}^{(1)}=0$ in the global equation, Eq. (14), whereas, for an impermeable top surface, $\bar{T}_q^{(1)}=0$ in Eq. (14).

4. ANALYSIS OF PAVEMENT-SOIL INTERACTION

The dynamic interaction between flexible pavement under moving load and multi-layered saturated soils is also examined in the present study. This soil-structure interaction problem was considered in the past for the cases of homogeneous elastic (Kim and Roesset 1998) and poroelastic (Cai *et al.* 2008) soils. In the present analysis, the pavement is modeled as an infinite elastic plate, and it behaves according to Kirchhoff small deflection thin plate theory. Consider a flexible plate resting on a multi-layered poroelastic half-space subjected to a moving load $P(x, y, t)$ applied to the plate as shown in Fig. 2. The contact surface between the plate and the supporting soil medium is assumed to be smooth, and the hydraulic boundary conditions at the contact surface can be either fully permeable or impermeable. The equation of motion of an elastic plate can be expressed as (Fryba 1972; Kim and McCullough 2003):

$$D_p\left[\frac{\partial^4 w_p(x,y,t)}{\partial x^4}+2\frac{\partial^4 w_p(x,y,t)}{\partial x^2\partial y^2}+\frac{\partial^4 w_p(x,y,t)}{\partial y^4}\right]+m_p\frac{\partial^2 w_p(x,y,t)}{\partial t^2}=P(x,y,t)+F(x,y,t) \tag{16}$$

where w_p denotes the plate deflection; $F(x, y, t)$ represents the reaction of the supporting soils applied to the plate; and m_p is the mass density of the plate per unit area. In addition, D_p is defined as the flexural rigidity of the plate and it is given by:

$$D_p=\frac{E_p h_p^3}{12(1-\nu_p^2)} \tag{17}$$

where E_p, h_p and ν_p are the Young's modulus, thickness and Poisson's ratio of the plate, respectively.

By applying the triple-dimensional Fourier transform to Eq. (16), the following equation can be obtained in the Fourier transform domain:

$$\left[D_p(k_x^2+k_y^2)^2-m_p\,\omega^2\right]\bar{w}_p(k_x,k_y,\omega)=\bar{P}(k_x,k_y,\omega)+\bar{F}(k_x,k_y,\omega) \tag{18}$$

The above equation can be solved by enforcing the continuity of vertical displacement and normal traction at the contact surface between the pavement and the supporting soil medium together with the hydraulic boundary conditions, which can be either fully permeable or impermeable. The exact stiffnes matrix scheme can be employed to obtain vertical displacements and pore pressure in

the supporting soil medium generated from the moving load applied to the pavement with different values of rigidity. For the case of impermeable pavement overlying multi-layered saturated soils, the following boundary conditions are to be satisfied in the global equation, Eq. (14):

$$\mathbf{u}^{(1)} = [\bar{u}_x^{(1)} \quad \bar{u}_y^{(1)} \quad \bar{w}_p \quad \bar{p}^{(1)}]^T \tag{19a}$$

$$\mathbf{T}^{(1)} = [0 \quad 0 \quad -\bar{F} \quad 0]^T \tag{19b}$$

$$\mathbf{T}^{(k)} = [0 \quad 0 \quad 0 \quad 0]^T, \quad k = 2, 3, \cdots, N+1 \tag{19c}$$

For flexible pavement with fully permeable contact surface, the continuity of traction and fluid flow at each layer interface given by Eq. (19c) remains unchanged, whereas the boundary conditions at the top surface of multi-layered saturated soils reduce to:

$$\mathbf{u}^{(1)} = [\bar{u}_x^{(1)} \quad \bar{u}_y^{(1)} \quad \bar{w}_p]^T \tag{20a}$$

$$\mathbf{T}^{(1)} = [0 \quad 0 \quad -\bar{F}]^T \tag{20b}$$

5. NUMERICAL RESULTS AND DISCUSSION

5.1 Numerical Solution Scheme

Numerical solution scheme based on the exact stiffness method outlined in the previous section is implemented into a computer program to investigate the dynamic response of multi-layered saturated soils to a moving load. In order to obtain the time domain solution, the numerical inversion of the triple-Fourier transform with the transform parameters k_x, k_y, and ω, given by Eq. (3b), must be performed. In this study, the time domain solutions are obtained by employing the fast Fourier transform (FFT), with the formula of FFT given by Brigham (1988). Equation (3b) can then be expressed as:

$$f(x, y, z, kT) = \frac{T_o}{N_t}\sum_{n=0}^{N-1}\left[\frac{1}{(2\pi)^2}\int_{-\infty}^{\infty}\int_{-\infty}^{\infty}\bar{f}\left(k_x, k_y, z, \frac{n}{N_t T}\right)e^{ik_x x + ik_y y}\,dk_x\,dk_y\right]e^{ink/N_t}, \quad k = 0, 1, \ldots, N_t - 1 \tag{21}$$

where N_t and T are defined as the sample number and the sample interval, respectively, in which $N_t = 2^r$ where r is an integer number, and $T = T_0/N_t$, where T_0 is the period of sample. The numerical evaluation of the double integrals in Eq. (21) is performed by using an adaptive numerical quadrature scheme proposed by Piessens *et al.* (1983), which subdivides the interval of integral and employs a 21-point Gauss-Kronrod rule to estimate the integral over each subinterval. In the present analysis, a moving load function $P(x, y, t)$ is given by Eq. (6) with the triple-Fourier transform being as shown in Eq. (8). In view of $\tilde{f}(\omega + k_x c)$ expressed in the form of Eq. (10) with the property of a Dirac delta function given by Eq. (7), the inverse Fourier transform with respect to the x-coordinate can then be obtained analytically by replacing x with $-(\omega - \omega_0)/c$. Subsequently, the double integral appearing in Eq. (21) is reduced to a single integral with respect to k_y.

5.2 Verification with Existing Solutions

The accuracy of the present solution scheme is verified with existing solutions for moving load problems. Figure 3 presents a comparison of time histories of normalized vertical displacement, $u_z^* = u_z a_R \mu_R / P_0$ where a_R is the reference length and μ_R is the reference shear modulus, at an observation point (0, 0, 1) under a point load P_0 moving with a constant velocity of 50 m/s on a homogeneous elastic half-space. The solutions from the present study are compared with the existing solutions given by Hung and Yang (2001). Note that the reference parameters employed by Hung and Yang (2001) are a_R = 1.0 m, $\mu_R = 1.0 \times 10^8$ N/m^2 and $\rho_R = 2.0 \times 10^3$ kg/m^3. The homogeneous half-space in the present study consists of ten soil layers of the same thickness $0.2a_R$ and an underlying half-space of identical material properties with very small values of poroelastic parameters (b, M, ρ_f, m and α are set to 10^{-3}). It is evident that the two solutions are in a very good agreement as shown in Fig. 3. A convergence study was also carried out, and it was found that numerically stable and converged solutions can be obtained with the number of a sample point of N_t = 4096 and the frequency number of $-8 \le \omega \le 8$.

Lu and Jeng (2007) examined dynamic response of a homogenous poroelastic half-space under a moving vertical point load P_0. Figure 4 presents the comparison of normalized vertical displacement u_z^* and normalized pore pressure $p^* = p/P_0$ between the present solutions and the solutions by Lu and Jeng (2007) at an observation point (x', 1, 1). Three cases of loading speed are investigated, which are $c = 0.1c_{SH}$, $c = 0.5c_{SH}$ and $c = 0.9c_{SH}$ where c_{SH} is the reference shear wave velocity, defined as $c_{SH} = \sqrt{\mu_R / \rho_R}$ where ρ_R is the reference density. In addition, a_R = 1.0 m, μ_R = 3.0 $\times 10^9$ N/m^2 and $\rho_R = 1.0 \times 10^3$ kg/m^3 in Lu and Jeng (2007). Note that the coordinates $-2 \le x' = x - ct \le 2$ and $y = z = 1$ are considered in the comparison. The comparison presented in Fig. 4 indicates a very good agreement between the two solutions for all velocities confirming the accuracy of proposed solution scheme.

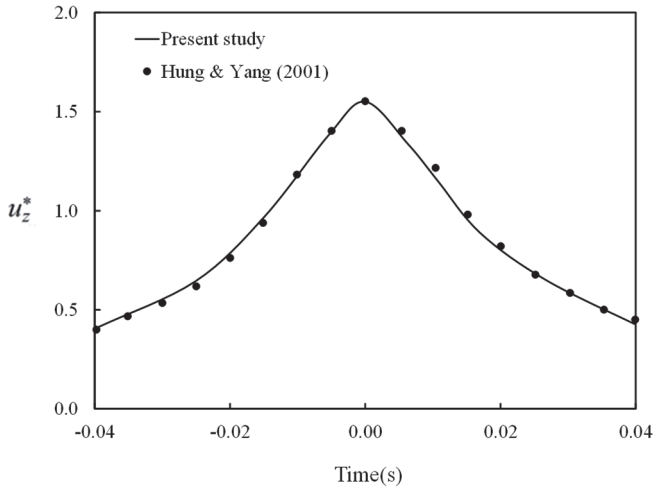

Fig. 3 Comparison of time histories of normalized vertical displacements at an observation point (0, 0, 1) induced by a moving point load with c = 50 m/s on a homogenous elastic half-space

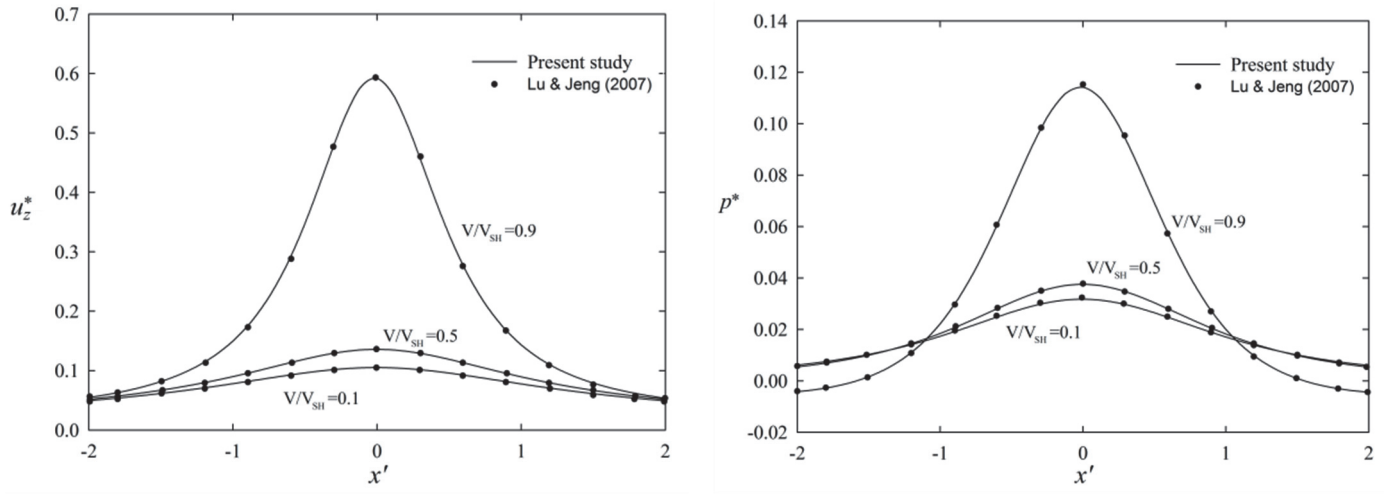

Fig. 4 Comparison results (a) normalized vertical displacement and (b) normalized pore pressure at an observation point (x', 1, 1) induced by a moving point load on a homogeneous poroelastic half-space

5.3 Numerical Solutions of Multi-Layered Saturated Soils under Moving Load

In this section, the dynamic response of multi-layered saturated soils under a moving point load is investigated. All length parameters are normalized with respect to a_R, *i.e.,* $x^* = x/a_R$, $y^* = y/a_R$, $z^* = z/a_R$. The time variable, the frequency and the velocity of loading are normalized as: $t^* = (t / a_R)\sqrt{\mu_R / \rho_R}$; $\omega^* = \omega_0 a_R \sqrt{\rho_R / \mu_R}$ and $c^* = c/c_{sh}$, respectively. In addition, other normalized material properties are defined as: $\lambda^* = \lambda/\mu_R$; $M^* = M/\mu_R$; $\rho_f^* = \rho_f/\rho_R$; $m^* = m/\rho_R$; and $b^* = a_R\, b / \sqrt{\rho_R\, \mu_R}$. Note that the reference parameters employed in all numerical results presented hereafter are chosen as follows: $a_R = 1.0$ m; $\mu_R = 2.5 \times 10^8$ N/m^2; and $\rho_R = 2.0 \times 10^3$ kg/m^3.

Consider a multi-layered poroelastic half-space underlying flexible pavement subjected to a moving point load P_0 as shown in Fig. 5. The multi-layered soil medium consists of two layers of the same thickness a_R and an underlying half-space. First, the numerical results corresponding to the multi-layered half-space under moving loads without an overlying plate are presented in Figs. 6 to 9 with three layered systems are considered, *i.e.,* system A, system B and system C. The material properties of the two layers and the half-space of system B are given in Table 1. For system C, the values of b are identical to those of system B except that $b^{(1)} = 1.2 \times 10^7$ N s/m^4. In addition, $b = 0$ in all layers of system A. Note that the influence of the parameter b is found to have the most significant influence on dynamic response of poroelastic soils under moving loads when compared to other poroelastic material parameters. (Theodorakopoulos 2003; Jin *et al.* 2004; Cai *et al.* 2007; 2008; Liu *et al.* 2017).

Figures 6 and 7, respectively present time histories of normalized vertical displacement and pore pressure at the depth $z/a_R = 1$ on the z-axis of the three poroelastic layer systems subjected to a moving point load with no oscillation ($\omega_0 = 0$) at the velocities of $0.5c_{sh}$ and $0.9c_{sh}$. It is found that both displacement and pore pressure in all systems are significantly influenced by the loading velocity. As expected, the highest peaks of both displacement and pore pressure are observed at the loading velocity of $0.9c_{sh}$. It is also found that the parameter b has more influence on the displacement at a higher velocity. In addition, excess pore pressure depends significantly on b at both velocities due to the fact that the

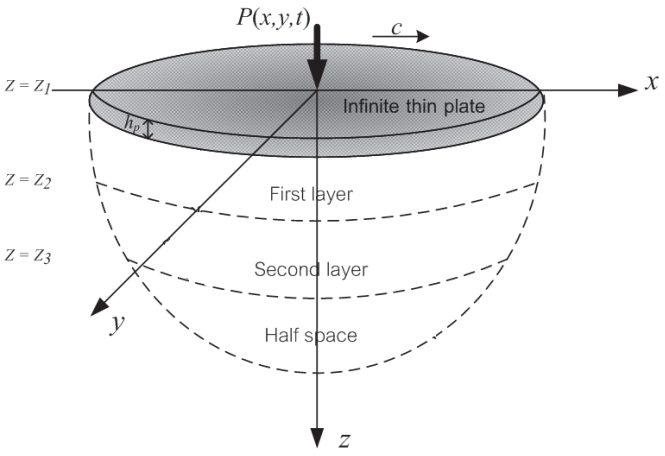

Fig. 5 Geometry of moving load problems considered in the numerical study

Table 1 Material properties of a multi-layered poroelastic half-space considered in the numerical study

	μ ($\times 10^8$ N/m^2)	λ ($\times 10^8$ N/m^2)	M ($\times 10^8$ N/m^2)	ρ ($\times 10^3$ kg/m^3)	ρ_f ($\times 10^3$ kg/m^3)	m ($\times 10^3$ kg/m^3)	α	b ($\times 10^6$ N s/m^4)
First layer	2.5	5	25	2	1	3	0.95	1.5
Second layer	1.25	1.88	18.8	1.6	1	1.8	0.98	0.75
Half-space	10	10	20	2.4	1	4.8	0.9	4.5

parameter b is inversely proportional to the permeability of the supporting soils with the soil medium being more permeable when the value of b becomes lower.

Figure 8 shows the profiles of normalized vertical displacement and normalized pore pressure along the z-axis at the time of $t^* = 0$ of the three systems of multi-layered saturated soils due to the moving point load. Numerical results presented in Fig. 8 reveal that the maximum vertical displacement occurs at the top surface of all layer systems at all loading speeds. Thereafter, the displacement decreases along the depth approaching a negligible value

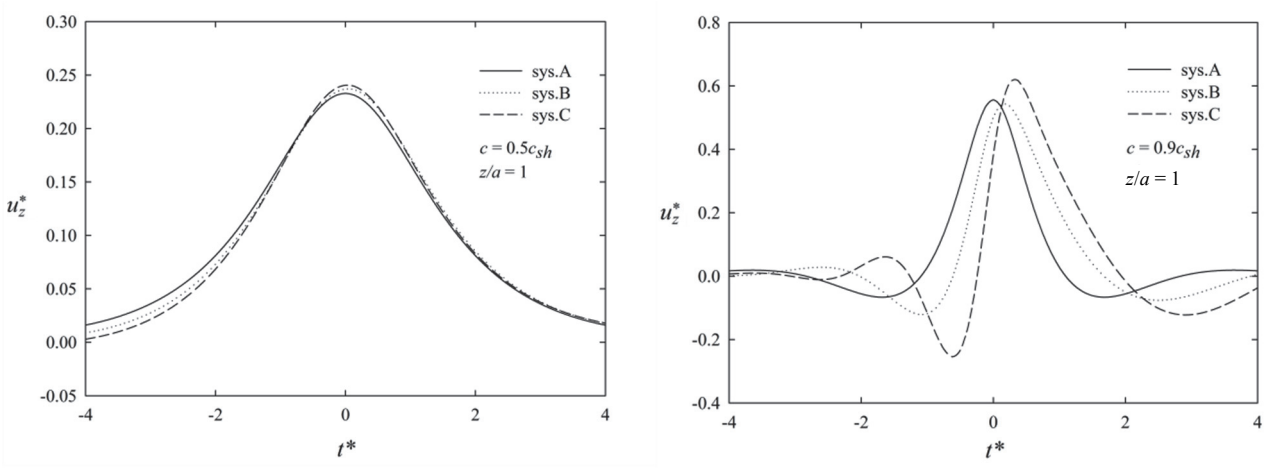

Fig. 6 Time histories of normalized vertical displacements at an observation point (0, 0, 1) of three multi-layered poroelastic soils due to a moving point load: (a) $0.5c_{sh}$ and (b) $0.9c_{sh}$

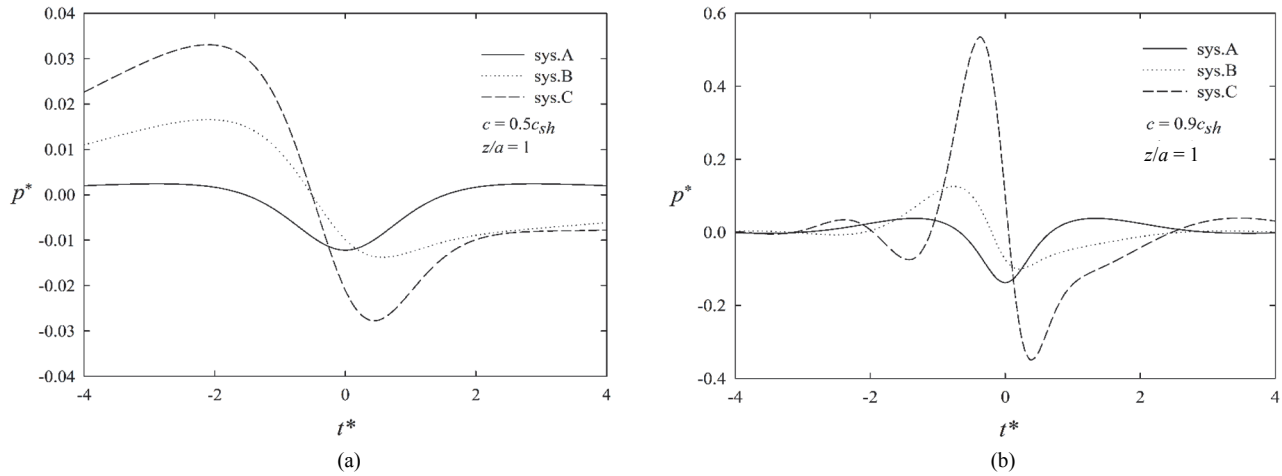

Fig. 7 Time histories of normalized pore pressure at an observation point (0, 0, 1) of three multi-layered poroelastic soils due to a moving point load: (a) $0.5c_{sh}$ and (b) $0.9c_{sh}$

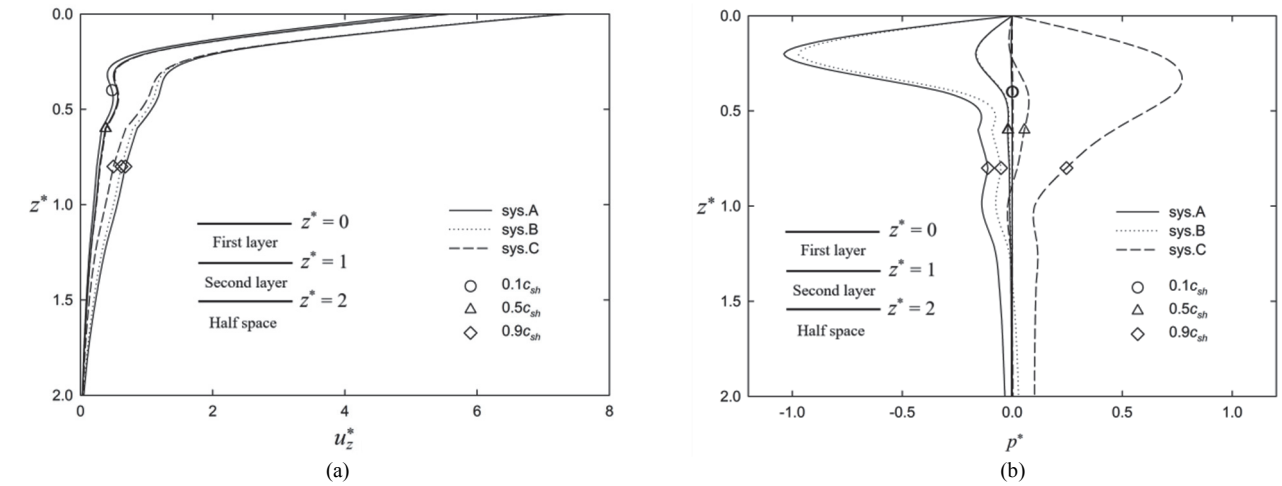

Fig. 8 Vertical profiles of (a) normalized vertical displacement; and (b) normalized pore pressure along the z-axis at $t^* = 0$ of three multi-layered poroelastic soils due to a moving point load in a moving reference frame

when $z^* > 2.0$. On the other hand, the pore pressure is zero at a fully permeable top surface. Thereafter, it immediately increases reaching the maximum value in the first layer, and then gradually decreases along the depth of all three saturated soils.

Figures 9(a) and 9(b), respectively, show the variation of normalized vertical displacement and normalized pore pressure with normalized oscillating frequency in the range of $0 \le \omega^* \le 2$ at the depth $z/a_R = 1$ on the z-axis. In addition, both normalized displacement and pore pressure in Fig. 9 are presented for the case of a point load moving at the velocity of $0.5c_{sh}$. It is observed from Fig. 9(a) that the displacement initially increases reaching the maximum value at $\omega^* \approx 0.6$ before it gradually decreases with increasing the oscillating frequency. Note that the highest peak of normalized displacement is found in the system A. The variation of pore pressure with the oscillating frequency presented in Fig. 9(b) indicates that initially it remains almost constant in the frequency range of $0 \le \omega^* \le 0.4$. Thereafter, the pore pressure increases with increasing frequency in all layer systems when $\omega^* > 0.6$.

5.4 Numerical Solutions of Pavement-Layered Soils Interaction under Moving Load

The final numerical results correspond to the case where flexible pavement, which is modeled as an infinite elastic plate overlying on a multi-layered poroelastic medium, is subjected to a moving point load as shown in Fig. 5. The contact surface between the plate and the supporting layered medium is assumed to be smooth and either fully permeable or impermeable. The material properties of the pavement are assigned as follows: $E_p = 3445 \times 10^6\ N/m^2$; $\nu_p = 0.35$; $h_p = 15.24$ cm and $m_p = 354$ kg/m^2 and the system B is chosen for the supporting layered soil. The different values of flexural rigidity of the plate D_p^* equal to 0.005, 0.01, 0.05, and 0.1 are considered where $D_p^* = D_p/\mu_R a_R^3$.

Vertical displacements in the layer system B underlying an infinite elastic plate subjected to a moving point load are illustrated next. The variations of normalized vertical displacements at the depth $z/a_R = 1$ on the z-axis of system B are plotted with respect to the loading velocity in Figs. 10(a) and 10(b) for fully permeable and impermeable plates, respectively. Vertical displacements show a notable dependence on the hydraulic boundary condition at the pavement-soil contact surface on the displacement especially at a higher velocity ($c^* > 0.8$). In addition, a higher displacement is observed in a fully permeable plate when compared to its impermeable counterpart. This is due to the fact that the water is not drained under an impermeable plate resulting in the excess pore pressure being developed in addition to the normal traction at the contact surface, which makes a layered soil stiffer under the impermeable hydraulic boundary condition.

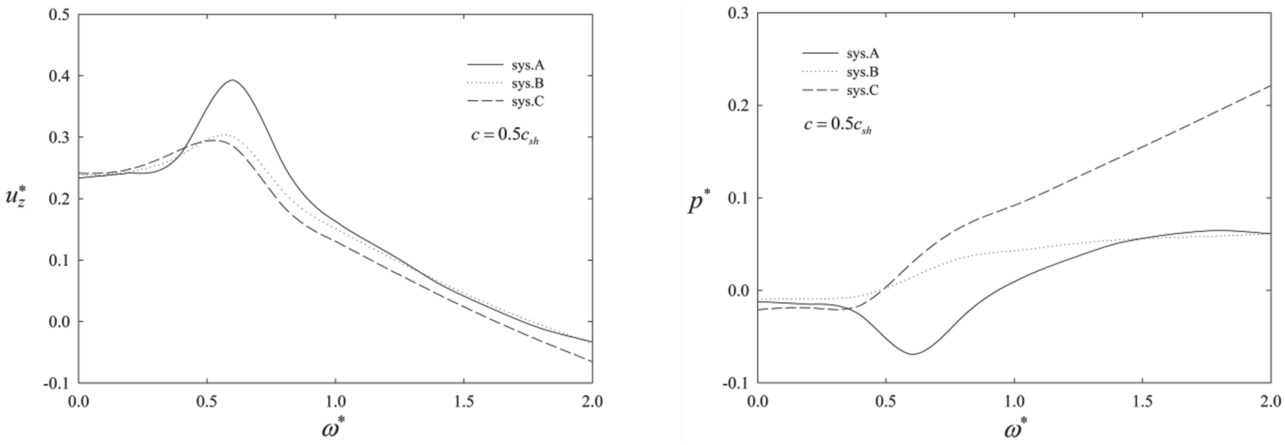

Fig. 9 Variations of (a) normalized vertical displacement; and (b) normalized pore pressure with oscillating frequencies at an observation point (0, 0, 1) of three multi-layered poroelastic soils due to a moving point load in a moving reference frame

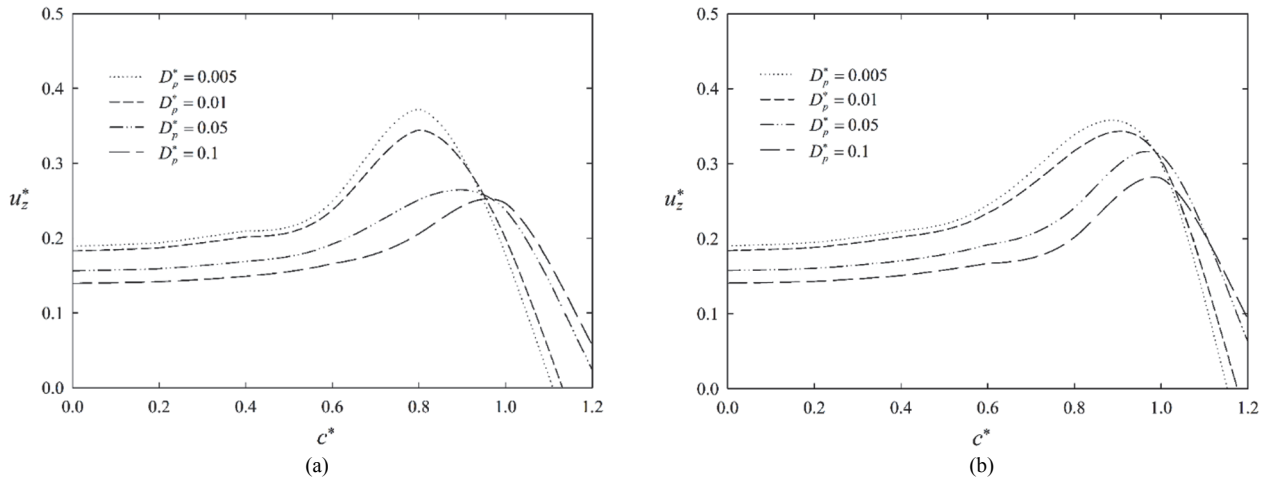

Fig. 10 Normalized vertical displacement at an observation point (0, 0, 1) of system B underlying infinite plate induced by a moving point load in a moving reference frame: (a) fully permeable plate and (b) fully impermeable plate

Numerical results presented in Fig. 10 also indicate that vertical displacements increase slowly in the range $0 \le c^* \le 0.5$ for both permeable and impermeable plates and all plate flexibilities. Thereafter, they rapidly increase reaching the peak values when $c^* > 0.8$. The earliest peak of displacements is found in the case of the plate with $D_p^* = 0.005$, followed by those with $D_p^* = 0.01$, 0.05 and 0.1, respectively. Figure 11 shows normalized excess pore pressure $p^* = pa_R^2/P_0$ at an observation point (0, 0, 0) of the layer system B underlying a fully impermeable plate induced by a moving point load in a moving reference frame. It is found that pore pressure decreases with the loading velocity for all plate flexibilities. It is also observed that excess pore pressure is reduced under a plate with more flexibility thus the maximum pore pressure occurs under the plate with $D_p^* = 0.005$ followed by $D_p^* = 0.01$, 0.05 and 0.1, respectively.

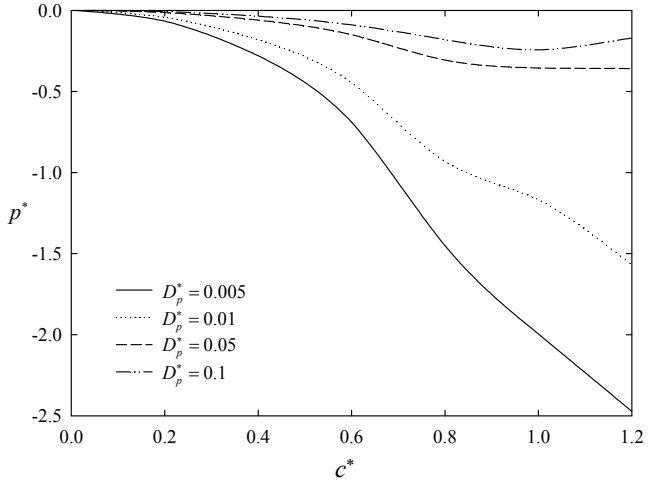

Fig. 11 Normalized pore pressure at an observation point (0, 0, 0) of system B underlying impermeable plate induced by a moving point load in a moving reference frame

6. CONCLUSIONS

In this paper, dynamic response of multi-layered saturated soils subjected to moving loads is successfully investigated by employing the exact stiffness matrix method. The layer stiffness matrices for the layered media are obtained from the analytical solutions derived in the frequency and wave number domains by using the triple-Fourier integral transform. Time domain solutions for a multi-layered poroelastic medium under moving loads are accurately determined by using the fast Fourier transform method and an adaptive numerical integration scheme. Numerical results on the multi-layered media under moving loads indicate that the influence of the parameter b, which represents the internal friction of a poroelastic material, on normalized displacement and pore pressure is more significant when the velocity of the moving load increases. It is also found from the analysis of flexible pavement-soil interaction under a moving point load that vertical displacements in multi-layered saturated soils depend significantly on the loading speed, the flexural rigidity of the pavement, and the hydraulic condition at the pavement-soil interface. The present solution scheme developed from the exact stiffness matrix method in this paper can be employed as the fundamental solutions in the development of semi-analytical numerical techniques for the analysis of more complicated soil-structure interaction problems involving moving loads such as underground tunnels in multi-layered saturated soils for high-speed trains.

ACKNOWLEDGEMENTS

The authors would like to thank the editor and reviewers for their careful reading and constructive comments useful to further enhance the quality of the paper.

FUNDING

The authors would like to acknowledge the support from Chulalongkorn University.

DATA AVAILABILITY

The data generated in this study are available from the corresponding author on reasonable request.

CONFLICT OF INTEREST STATEMENT

The authors declare that they have no known potential conflicts of interest, including financial interests (such as funding source, employment or consultancy with a private company, honoraria, etc.) and non-financial interests (such as personal or professional relationship, academic competition, religious view, etc.) that could affect editor's, reviewer's and readers' objectivity inappropriately

NOTATIONS

a	Length (m)
a_R	Reference length (m)
b	Parameter accounting for the internal friction of the medium (N·s/m^4)
c	Velocity of the moving load (m/s^2)
c_{sh}	Reference shear wave velocity (m/s^2)
D_p	Flexural rigidity of the plate (N/m^2)
E_p	Young's modulus of the plate (N/m^2)
h_p	Thickness of a plate (m)
k_x, k_y	Wave numbers associated with the x and y coordinates
$\mathbf{K}^{(n)}$	Stiffness matrix of the nth layer
$\mathbf{K}^{(N+1)}$	Stiffness matrix of the underlying half-space
m	Density-like parameter (kg/m^3)
m_p	Mass density of the plate per unit area (kg/m^2)
p	Excess pore fluid pressure (N/m^2)
$P(x, y, t)$	Function of the moving load
q_i	Fluid discharge in the i-direction (m^3/s)
t	Time variable (s)
u_i	Displacement of the solid matrix in the i-direction (m)
v_p	Poisson's ratio of the plate
w_i	Fluid displacement relative to the solid matrix in the i-direction (m)
w_p	Plate deflection (m)
x, y, z	Cartesian coordinates (m)
α	Biot's parameters accounting for compressibility of the medium
M	Biot's parameters accounting for compressibility of the medium (N/m^2)
δ	Dirac delta function
ε_{ij}	Strain component of the solid matrix
μ, λ	Lame' constants (N/m^2)

μ_R	Reference shear modulus (N/m^2)
ρ	Mass densities of the bulk material (kg/m^3)
ρ_f	Mass densities of the pore fluid (kg/m^3)
σ_{ij}	Total stress component the bulk material (N/m^2)
ω	Frequency (kg/m^3)
z	depth (m)

REFERENCES

Ai, Z.Y., Mu, J.J., and Ren, G.P. (2018). "3D dynamic response of a transversely isotropic multilayered medium subjected to a moving load." *International Journal for Numerical and Analytical Methods in Geomechanics*, **42**(4), 636-654. https://doi.org/10.1002/nag.2758

Ai, Z.Y. and Ren, G.P. (2016). "Dynamic analysis of a transversely isotropic multilayered half-plane subjected to a moving load." *Soil Dynamics and Earthquake Engineering*, **83**, 162-166. https://doi.org/10.1016/j.soildyn.2016.01.022

Ai, Z.Y. and Wang, L.H. (2017). "Effect of compressible parameters on vertical vibration of an elastic pile in multilayered poroelastic media." *Computers and Geotechnics*, **89**, 195-202. https://doi.org/10.1016/j.compgeo.2017.05.002

Barros, F.C.P. and Luco, J.E. (1994). "Response of a layered viscoelastic half-space to a moving point load." *Wave Motion*, **19**, 189-210. https://doi.org/10.1016/0165-2125(94)90066-3

Biot, M.A. (1941). "General theory of three-dimensional consolidation." *Journal of Applied Physics*, **12**, 155-164.

Biot, M.A. (1956). "Theory of propagation of elastic waves in a fluid-saturated porous solid, part I: Low-frequency range." *The Journal of the Acoustical Society of America*, **28**, 168-178.

Biot, M.A. (1962). "Mechanics of deformation and acoustic propagation in porous media." *Journal of Applied Physics*, **33**, 1482-1498.

Brigham, E.O. (1988). *The Fast Fourier Transform and Its Applications*. Prentice-Hall, New Jersey.

Burke, M. and Kingsbury, H.B. (1984). "Response of poroelastic layers to moving loads." *International Journal of Solids and Structures*, **20**, 499-511. https://doi.org/10.1016/0020-7683(84)90015-5

Cai, Y., Chen, Y., Cao, Z., Sun, H., and Guo, L. (2015). "Dynamic responses of a saturated poroelastic half-space generated by a moving truck on the uneven pavement." *Soil Dynamics and Earthquake Engineering*, **69**, 172-181. https://doi.org/10.1016/j.soildyn.2014.10.014

Cai, Y., Sun, H., and Xu, C. (2007). "Steady state responses of poroelastic half-space soil medium to a moving rectangular load." *International Journal of Solids and Structures*, **44**, 7183-7196. https://doi.org/10.1016/j.ijsolstr.2007.04.006

Cai, Y., Sun, H., and Xu, C. (2008). "Three dimensional analysis of dynamic responses of track ground system subjected to a moving train load." *Computers and Structures*, **86**, 816-824. https://doi.org/10.1016/j.compstruc.2007.07.001

Eason, G. (1965). "The stress produced in a semi-infinite solid by moving surface force." *International Journal of Engineering Science*, **2**, 581-609. https://doi.org/10.1016/0020-7225(65)90038-8

Fryba, L. (1972). *Vibration of Solids and Structures Under Moving Loads*. Noordhoff International, The Netherlands.

Grundmann, H., Lieb, M., and Trommer, E. (1999). "The response of a layered half-space to traffic loads moving along its surface." *Archive of Applied Mechanics*, **69**, 55-67. https://doi.org/10.1007/s004190050204

Hu, A.F., Peng, F., Xia, C.Q., and Xie, K.H. (2017). "Lateral dynamic response of a partially embedded pile subjected to combined loads in saturated soil." *Marine Georesources and Geotechnology*, **35**(6), 788-798. https://doi.org/10.1080/1064119X.2016.1240276

Hung, H.H. and Yang, Y.B. (2001). "Elastic waves in visco-elastic half-space generated by various vehicle loads." *Soil Dynamics and Earthquake Engineering*, **21**, 1-17. https://doi.org/10.1016/S0267-7261(00)00078-6

Jin, B., Yue, Z.Q., and Tham, L.G. (2004). "Stresses and excess pore pressure induced in saturated poroelastic half space by moving line load." *Soil Dynamics and Earthquake Engineering*, 24, 25-33. https://doi.org/10.1016/j.soildyn.2003.09.004

Jones, D.V., Laghrouche, O., Le Houe´dec, D., and Petyt, M. (1997). "Ground vibration in the vicinity of a rectangular load acting on a viscoelastic layer over a rigid foundation." *Journal of Sound and Vibration*, **203**(2), 307-319. https://doi.org/10.1006/jsvi.1996.0899

Kaewjuea, W., Senjuntichai, T., and Rajapakse, R.K.N.D. (2014). "Dynamic response of borehole in poroelastic medium with disturbed zone." *CMES: Computer Modeling in Engineering and Sciences*, **101**, 207-228. https://doi.org/10.3970/cmes.2014.101.207

Keer, L.M. (1969). "Moving and simultaneously fluctuating loads on an elastic half-plane." *The Journal of the Acoustical Society of America*, **47**, 1359-1365.

Kim, S.M. and Roesset, J.M. (1998). "Moving loads on a plate on elastic foundation." *Journal of Engineering Mechanics*, ASCE, **124**(9). https://doi.org/10.1061/(ASCE)0733-9399(1998)124:9(1010)

Kim, S.M. and McCullough, B.F. (2003). "Dynamic response of plate on viscous Winkler foundation to moving loads of varying amplitude." *Engineering Structures*, **25**, 1179-1188. https://doi.org/10.1016/S0141-0296(03)00066-X

Lefeuve-Mesgouez, G. and Mesgouez, A. (2012). "Three-dimensional dynamic response of a porous multilayered ground under moving loads of various distributions." *Advances in Engineering Software*, **46**, 75-84. https://doi.org/10.1016/j.advengsoft.2010.09.006

Lefeuve-Mesgouez, G., Peplow, A.T., and Le Houédec, D. (2002). "Surface vibration due to a sequence of high speed moving harmonic rectangular loads." *Soil Dynamics and Earthquake Engineering*, **22**(6), 459-473. https://doi.org/10.1016/S0267-7261(02)00034-9

Liu, B., Su, Q., Liu, T., and Li, T. (2017). "Dynamic response of water saturated subgrade surface layer under high speed train using moving element method." *Journal of Vibroengineering*, **19**(5), 3720-3736. https://doi.org/10.21595/jve.2017.18187

Lu, J.F. and Jeng, D.S. (2007). "A half-space saturated poro-elastic medium subjected to a moving point load." *International Journal of Solids and Structures*, **44**, 573-586. https://doi.org/10.1016/j.ijsolstr.2006.05.020

Piessens, R., Doncker-Kapenga, E., Uberhuber, C.W., and Kahaner, D.K. (1983) *QUADPACK, A Subroutine Package for Automatic Integration*, Springer, Berlin.

Senjuntichai, T. and Kaewjuea, W. (2008). "Dynamic response of multiple flexible strips on a multilayered poroelastic half-plane." *Journal of Mechanics of Materials and Structures*, **3**(10), 1885-1901. https://doi.org/10.2140/jomms.2008.3.1885

Senjuntichai, T., Keawsawasvong, S., and Plangmal, R. (2018). "Vertical vibrations of rigid foundations of arbitrary shape in a multi-layered poroelastic medium." *Computers and Geotechnics*, **100**, 121-134.

https://doi.org/10.1016/j.compgeo.2018.04.012

Senjuntichai, T., Keawsawasvong, S., and Plangmal, R. (2019). "Three-dimensional dynamic response of multi-layered poroelastic media." *Marine Georesources and Geotechnology*, **37**(4), 424-437. https://doi.org/10.1080/1064119X.2018.1446200

Si, L.T., Zhao, Y., Zhang, Y.H., and Kennedy, D. (2016). "A hybrid approach to analyse a beam-soil structure under a moving random load." *Journal of Sound and Vibration*, **382**, 179-192. https://doi.org/10.1016/j.jsv.2016.07.012

Siddharthan, R., Zafir, Z., and Norris, G.M. (1993). "Moving load response of layered soil. I. Formulation." *Journal of Engineering Mechanics*, ASCE, **119**, 2052-2071. https://doi.org/10.1061/(ASCE)0733-9399(1993)119:10(2052)

Sneddon, I.N. (1952). "The stresses produced by a pulse of pressure moving along the surface of a semi-infinite solid." *Rendiconti del Circolo Matematico di Palermo*, **2**, 57-62.

Theodorakopoulos, D.D. (2003). "Dynamic analysis of a poroelastic half-plane soil medium under moving loads." *Soil Dynamics and Earthquake Engineering*, **23**(7), 521-533. https://doi.org/10.1016/S0267-7261(03)00074-5

Xu, B., Lu, J.F., and Wang, J.H. (2008). "Dynamic response of a layered water-saturated halfspace to a moving load." *Computers and Geotechnics*, **35**, 1-10. https://doi.org/10.1016/j.compgeo.2007.03.005

Zeng, X. and Rajapakse, R.K.N.D. (1999). "Vertical vibrations of a rigid disk embedded in a poroelastic medium." *International Journal for Numerical and Analytical Methods in Geomechanics*, **23**(15), 2075-2095. https://doi.org/10.1002/(SICI)1096-9853(19991225)23:15<2075::AID-NAG50>3.0.CO;2-P

APPENDIX

Explicit expressions of the elements of $\mathbf{K}^{(n)}$ (Senjuntichai *et al.* 2019)

1st row:

$$k_{11} = \frac{\mu}{R_l}\{8(a_1-a_2)k_y^2\,\alpha_{3n}\,\gamma_3^2\,\Gamma_3\,\psi_{32} + \gamma_3\left[k_y^2\,\Gamma_1-(k_x^2-\gamma_3^2)\,\Gamma_{11}\right]\Gamma_{13}\,\psi_{32} + 2(k_x^2-\gamma_3^2)\,\Gamma_4\,\Gamma_{12}\,\psi_{31}\,\psi_{32} + (a_1-a_2)\,\Gamma_2(S^2\,k_x^2\,\psi_{31}^2-2k_y^2\,\gamma_3^2\,\psi_{32}^2)\} \quad (A.1)$$

$$k_{12} = \frac{\mu}{R_l}\{-8(a_1-a_2)k_x\,k_y\,\alpha_{3n}\,\gamma_3^2\,\Gamma_3\,\psi_{32} - k_x\,k_y\,\gamma_3(\Gamma_1+\Gamma_{11})\,\Gamma_{13}\,\psi_{32} + 2k_x\,k_y\,\Gamma_4\,\Gamma_{12}\,\psi_{31}\,\psi_{32} + (a_1-a_2)\,k_x\,k_y\,\Gamma_2\left[k^2\psi_{31}^2+\gamma_3^2(-4+4\psi_{32}+\psi_{32}^2)\right]\} \quad (A.2)$$

$$k_{13} = \frac{\mu\psi_{31}}{R_l}\{-4(a_1-a_2)\,k_x\,\alpha_{3n}\,\gamma_3(3k^2+\gamma_3^2)\,\Gamma_3 - k_x\left[(k^2+\gamma_3^2)\,\Gamma_1+2\gamma_3^2\,\Gamma_{11}\right]\Gamma_{13} + 4k_x\,\gamma_3\,\Gamma_4\Gamma_{12}\,\psi_{31} + (a_1-a_2)\,k_x\,\gamma_3(3k^2+\gamma_3^2)\,\Gamma_2\,\psi_{32}\} \quad (A.3)$$

$$k_{14} = -\frac{S^2\mu a_1\,a_2\,k_x\,\psi_{31}}{R_l}\{(a_1-a_2)\,k^2(\gamma_1\,\psi_{12}\,\psi_{21} - \gamma_2\,\psi_{11}\,\psi_{22})\,\psi_{31} - (a_1\,\gamma_1^2+a_2\,\gamma_2^2)\,\gamma_3\,\psi_{11}\,\psi_{21}\,\psi_{32} + 4\alpha_{1n}\,\gamma_1\,\gamma_2\,\gamma_3\left[a_2(\alpha_{3n}\,\psi_{22}-\alpha_{2n}\,\psi_{32}) - a_1\,(\alpha_{3n}\,\psi_{22}+\alpha_{2n}\,\psi_{32}) + \gamma_1\,\gamma_2\,\gamma_3\,\psi_{12}\left[a_2\,\Gamma_6 + a_1(4\alpha_{2n}\,\alpha_{3n}+\psi_{22}\,\psi_{32})\right]\right]\} \quad (A.4)$$

$$k_{15} = \frac{\mu}{R_l}\{2\alpha_{3n}\,\gamma_3\left[-k_y^2\,\Gamma_1+(k_x^2-\gamma_3^2)\,\Gamma_{11}\right]\Gamma_{13} + 4\alpha_{3n}(-k_x^2+\gamma_3^2)\,\Gamma_4\,\Gamma_{12}\,\psi_{31} - 2(a_1-a_2)\,\Gamma_3(8k_y^2\,\alpha_{3n}^2\,\gamma_3^2+S^2\,k_x^2\,\psi_{31}^2) + 4(a_1-a_2)\,k_y^2\,\alpha_{3n}\,\gamma_3^2\,\Gamma_2\,\psi_{32}\} \quad (A.5)$$

$$k_{16} = \frac{\mu}{R_l}\{2k_x\,k_y\,\alpha_{3n}\,\gamma_3(\Gamma_1+\Gamma_{11})\,\Gamma_{13} - 4k_x\,k_y\,\alpha_{3n}\,\Gamma_4\,\Gamma_{12}\,\psi_{31} - 4(a_1-a_2)\,k_x\,k_y\,\alpha_{3n}\,\gamma_3^2\,\Gamma_2\,\psi_{32} - 2(a_1-a_2)\,k_x\,k_y\,\Gamma_3\left[k^2\,\psi_{31}^2-\gamma_3^2(-4+4\psi_{32}+\psi_{32}^2)\right]\} \quad (A.6)$$

$$k_{17} = \frac{2S^2\mu(a_1-a_2)\,k_x\,\gamma_3\,\psi_{31}}{R_l}\{a_1\,\gamma_1\,\psi_{21}(-\alpha_{3n}\,\psi_{12} + \alpha_n\,\psi_{32}) + a_2\,\gamma_2\,\psi_{11}(\alpha_{3n}\,\psi_{22}-\alpha_{2n}\,\psi_{32})\} \quad (A.7)$$

$$k_{18} = -\frac{\mu\psi_{31}}{R_l}\{2S^2 a_1\,a_2\,k_x\,\alpha_{3n}\,\gamma_3\left[-(a_1+a_2)\,\gamma_1\,\gamma_2\,\Gamma_4 + (a_1\,\gamma_1^2+a_2\,\gamma_2^2)\,\psi_{11}\,\psi_{21}\right] + 2S^2(a_1-a_2)\,k_x\left[-a_1\,a_2\,k^2(-\alpha_{2n}\,\gamma_2\,\psi_{11} + \alpha_{1n}\,\gamma_1\,\psi_{21})\,\psi_{31} + \Gamma_{12}(-\alpha_{2n}\,\psi_{12}+\alpha_{1n}\,\psi_{22})\psi_{32}\right]\} \quad (A.8)$$

2nd row:

$$k_{22} = \frac{\mu}{R_l}\{8(a_1-a_2)\,k_x^2\,\alpha_{3n}\,\gamma_3^2\,\Gamma_3\,\psi_{32} + \gamma_3\left[k_x^2\,\Gamma_1-(k_y^2-\gamma_3^2)\,\Gamma_{11}\right]\Gamma_{13}\,\psi_{32} + 2(k_y^2-\gamma_3^2)\,\Gamma_4\,\Gamma_{12}\,\psi_{31}\,\psi_{32} + (a_1-a_2)\,\Gamma_2(S^2\,k_y^2\,\psi_{31}^2-2k_x^2\,\gamma_3^2\,\psi_{32}^2)\} \quad (A.9)$$

$$k_{23} = \frac{k_y}{k_x}k_{13}, \quad k_{24} = \frac{k_y}{k_x}k_{14}, \quad k_{25} = k_{16} \quad (A.10)$$

$$k_{26} = \frac{\mu}{R_l}\{-2\alpha_{3n}\,\gamma_3\left[k_x^2\,\Gamma_1-(k_y^2-\gamma_3^2)\,\Gamma_{11}\right]\Gamma_{13} - 4\alpha_{3n}(k_y^2-\gamma_3^2)\,\Gamma_4\,\Gamma_{12}\,\psi_{31} - 2(a_1-a_2)\,\Gamma_3(8k_x^2\,\alpha_{3n}^2\,\gamma_3^2+S^2\,k_y^2\,\psi_{31}^2) + 4(a_1-a_2)\,k_x^2\,\alpha_{3n}\,\gamma_3^2\,\Gamma_2\,\psi_{32}\} \quad (A.11)$$

$$k_{27}=\frac{k_y}{k_x}k_{17}\,,\quad k_{28}=\frac{k_y}{k_x}k_{18} \tag{A.12}$$

3rd row:

$$k_{33}=\frac{\mu\Gamma_7}{R_l}\left[-\gamma_3\,\Gamma_2\,\psi_{31}+(a_1-a_2)\,k^2\,\psi_{11}\,\psi_{21}\,\psi_{32}\right] \tag{A.13}$$

$$\begin{aligned}k_{34}=\frac{\mu\psi_{31}}{R_l}\Big\{&\left[(a_1-a_2)(-a_2\,g_3+a_1\,g_4)k^4+a_1^2(g_4+2a_2\,k^2)\,\gamma_1^2\,\gamma_3^2+a_2^2(g_3+2a_1\,k^2)\,\gamma_2^2\gamma_3^2\right]\Gamma_{13}\\&-a_2k^2\left[2a_2g_3-a_1(g_3+g_4)-2a_1(a_1-a_2)k^2\right]\gamma_2\,\gamma_3\,\Gamma_6\,\psi_{11}\\&-a_1k^2\left[2a_1g_4-a_2(g_3+g_4)+2(a_1-a_2)a_2\,k^2\right]\gamma_1\,\gamma_3\,\Gamma_5\,\psi_{21}-\left[g_3+g_4+2(a_1+a_2)k^2\right]\gamma_3\,\Gamma_4\,\Gamma_{12}\,\psi_{31}\Big\}\end{aligned} \tag{A.14}$$

$$k_{35}=-\frac{2\mu k_x\,\Gamma_7}{R_l}\left[a_1\,\gamma_1\,\psi_{21}(-\alpha_{3n}\,\psi_{12}+\alpha_{1n}\,\psi_{32})+a_2\,\gamma_2\,\psi_{11}(\alpha_{3n}\,\psi_{22}-\alpha_{2n}\,\psi_{32})\right] \tag{A.15}$$

$$k_{36}=\frac{k_y}{k_x}k_{35} \tag{A.16}$$

$$k_{37}=-\frac{2\mu}{R_l}\left[g_3-g_4+2(a_1-a_2)k^2\right]\gamma_3\,\psi_{31}\left[(a_1-a_2)k^2\alpha_{3n}\,\psi_{11}\,\psi_{21}-\gamma_3\,\Gamma_3\,\psi_{31}\right] \tag{A.17}$$

$$k_{38}=\frac{2\mu a_1\,a_2\,\Gamma_7}{R_l}\left\{-k^2\,\gamma_2\,\psi_{11}(-\alpha_{3n}\,\psi_{22}+\alpha_{2n}\,\psi_{32})+\gamma_1\left[\gamma_2\,\gamma_3(\alpha_{2n}\,\psi_{12}-\alpha_{1n}\,\psi_{22})\,\psi_{31}+k^2\,\psi_{21}(-\alpha_{3n}\,\psi_{12}+\alpha_{1n}\,\psi_{32})\right]\right\} \tag{A.18}$$

4th row:

$$\begin{aligned}k_{44}=-\frac{\psi_{31}}{R_l}\Big\{&-4a_2\,k^2\,\alpha_{2n}\,\alpha_{3n}\left[2a_2\,h_1\,\gamma_2+\vartheta a_1^2\,\gamma_1\,\gamma_2-a_1\left(h_2\,\gamma_1+(h_1+\vartheta a_2\,\gamma_1)\gamma_2\right)\right]\gamma_3\,\psi_{12}\\&-4a_1k^2\alpha_{1n}\alpha_{3n}\gamma_3\left[a_1\gamma_1(h_2+\Gamma_{10})+a_2(-h_1\gamma_2-\gamma_1\Gamma_{10})\right]\psi_{22}+(-a_1h_2\gamma_1+a_2h_1\,\gamma_2)\,\gamma_3^2(-a_2\,\gamma_2\,\psi_{12}\,\psi_{21}+a_1\,\gamma_1\,\psi_{11}\,\psi_{22})\,\psi_{31}\\&+(a_1-a_2)k^4\left[(a_2\,h_1\,\psi_{12}\,\psi_{21}-a_1\,h_2\,\psi_{11}\,\psi_{22})\psi_{31}+\vartheta a_1\,a_2(-\gamma_1\,\psi_{12}\,\psi_{21}+\gamma_2\,\psi_{11}\,\psi_{22})\psi_{31}\right]\\&+a_1\,a_2\,k^2\,\gamma_3\left[-4\alpha_{1n}\,\alpha_{2n}(\gamma_2\,\Gamma_9+\gamma_1\,\Gamma_{10})+(-\gamma_1\,\Gamma_9-\gamma_2\,\Gamma_{10})\psi_{11}\,\psi_{21}\right]\psi_{32}+k^2\,\gamma_3\,\Gamma_8\,\psi_{12}\,\psi_{22}\,\psi_{32}\Big\}\end{aligned} \tag{A.19}$$

$$\begin{aligned}k_{45}=-\frac{\psi_{31}}{R_l}\Big[&2k_x\,\alpha_{3n}\,\gamma_3(-a_1\,\gamma_1\,\Gamma_9-a_2\,\gamma_2\,\Gamma_{10})\,\psi_{11}\,\psi_{21}+2k_x\,\alpha_{3n}\,\gamma_3(a_2\,\gamma_2\,\Gamma_9+a_1\,\gamma_1\,\Gamma_{10})(-4\alpha_n\,\alpha_{2n}+\psi_{12}\,\psi_{22})\\&+2(a_1-a_2)\,k_s\,k_x(-\alpha_{2n}\,\Gamma_{10}\,\psi_{11}+\alpha_{1n}\,\Gamma_9\,\psi_{21})\,\psi_{31}-2k_x(a_1\,h_2\,\gamma_1-a_2\,h_1\,\gamma_2)\gamma_3(-\alpha_{2n}\,\psi_{12}+\alpha_{1n}\,\psi_{22})\,\psi_{32}\Big]\end{aligned} \tag{A.20}$$

$$k_{46}=\frac{k_y}{k_x}k_{45} \tag{A.21}$$

$$\begin{aligned}k_{47}=\frac{\psi_{31}}{R_l}\Big[&-2(a_1\,h_2\,\gamma_1-a_2\,h_1\,\gamma_2)\,\gamma_3^2(-\alpha_{2n}\,\psi_{12}+\alpha_{1n}\,\psi_{22})\,\psi_{31}\\&-2(a_1-a_2)k^2\,\gamma_3\,\Gamma_9\,\psi_{21}(\alpha_{3n}\,\psi_{12}-\alpha_n\,\psi_{32})-2(a_1-a_2)k^2\,\gamma_3\,\Gamma_{10}\,\psi_{11}(-\alpha_{3n}\,\psi_{22}+\alpha_{2n}\,\psi_{32})\Big]\end{aligned} \tag{A.22}$$

$$\begin{aligned}k_{48}=-\frac{\psi_{31}}{R_l}\Big\{&8k^2\,\alpha_{1n}\,\alpha_{2n}\,\alpha_{3n}\,\gamma_3\,\Gamma_8-2a_1\,\alpha_{2n}\left[-a_1\,h_2\,\gamma_1^2\,\gamma_3^2+a_2\,h_1\,\gamma_1\,\gamma_2\,\gamma_3^2-(a_1-a_2)\,k^4\,\Gamma_{10}\right]\psi_{11}\psi_{31}\\&+2a_2\,\alpha_n\left[\vartheta a_1^2\,k^4\,\gamma_1-a_1\left(k^4(h_1+\vartheta a_2\,\gamma_1)+h_2\,\gamma_1\,\gamma_2\,\gamma_3^2\right)+a_2\,h_1(k^4+\gamma_2^2\,\gamma_3^2)\right]\psi_{21}\,\psi_{31}\\&+2a_2\,k^2\,\gamma_3\left[a_1\,\alpha_{3n}(\gamma_1\,\Gamma_9+\gamma_2\,\Gamma_{10})\psi_{11}\,\psi_{21}+\alpha_{1n}\left(-2a_2\,h_1\,\gamma_2+\vartheta a_1(-a_1+a_2)\gamma_1\gamma_2+a_1(h_2\gamma_1+h_1\gamma_2)\right)\psi_{22}\psi_{32}\right]\\&+2a_1\,k^2\gamma_3\,\psi_{12}\left[a_2(h_1\,\gamma_2+\gamma_1\,\Gamma_{10})(-\alpha_{3n}\,\psi_{22}+\alpha_{2n}\,\psi_{32})+a_1\,\gamma_1\left(-2h_2\,\alpha_{2n}\,\psi_{32}+\vartheta a_2\,\gamma_2(\alpha_{3n}\,\psi_{22}+\alpha_{2n}\,\psi_{32})\right)\right]\Big\}\end{aligned} \tag{A.23}$$

5th row:

$$k_{55} = k_{11}\ ;\quad k_{56} = k_{12}\ ;\quad k_{57} = -k_{13}\ ;\quad k_{58} = k_{14} \tag{A.24}$$

6th row:

$$k_{66} = k_{22}\ ;\quad k_{67} = -k_{23}\ ;\quad k_{68} = k_{24} \tag{A.25}$$

7th row:

$$k_{77} = k_{33}\ ;\ k_{78} = -k_{34} \tag{A.26}$$

8th row:

$$k_{88} = k_{44} \tag{A.27}$$

where

$$R_l = \psi_{31}\left\{\left[2a_1 a_2 k^4 - a_1^2(k^4+\gamma_1^2\gamma_3^2) - a_2^2(k^4+\gamma_2^2\gamma_3^2)\right]\Gamma_{13} - 2(a_1-a_2)\,a_2 k^2\gamma_2\gamma_3\Gamma_6\psi_{11} + 2a_1(a_1-a_2)\,k^2\gamma_1\gamma_3\Gamma_5\psi_{21} + 2\gamma_3\Gamma_4\Gamma_{12}\psi_{31}\right\} \tag{A.28}$$

$$\alpha_{in} = e^{-\gamma_i h_n}\quad ;\quad i = 1,2,3\ ;\ n = 1,2,\ldots,N \tag{A.29}$$

$$\psi_{ij} = (-1)^j + \alpha_{in}^2;\ i = 1,2,3\ ;\ j = 1,2 \tag{A.30}$$

$$\Gamma_1 = (a_1 - a_2)^2 k^2 \tag{A.31}$$

$$\Gamma_2 = a_1\gamma_1\psi_{12}\psi_{21} - a_2\gamma_2\psi_{11}\psi_{22} \tag{A.32}$$

$$\Gamma_3 = -a_2\alpha_{2n}\gamma_2\psi_{11} + a_1\alpha_n\gamma_1\psi_{21} \tag{A.33}$$

$$\Gamma_4 = -4\alpha_n\alpha_{2n} + \psi_{12}\psi_{22} \tag{A.34}$$

$$\Gamma_5 = -4\alpha_n\alpha_{3n} + \psi_{12}\psi_{32} \tag{A.35}$$

$$\Gamma_6 = -4\alpha_{2n}\alpha_{3n} + \psi_{22}\psi_{32} \tag{A.36}$$

$$\Gamma_7 = \left[g_3 - g_4 + 2(a_1-a_2)(k_x^2+k_y^2)\right]\gamma_3\psi_{31} \tag{A.37}$$

$$\Gamma_8 = 2a_2^2 h_1\gamma_2 + a_1^2\gamma_1(2h_2 - \vartheta a_2\gamma_2) - a_1 a_2\left[h_2\gamma_1 + (h_1 + \vartheta a_2\gamma_1)\gamma_2\right] \tag{A.38}$$

$$\Gamma_9 = h_1 - \vartheta a_1\gamma_1 \tag{A.39}$$

$$\Gamma_{10} = h_2 - \vartheta a_2\gamma_2 \tag{A.40}$$

$$\Gamma_{11} = a_1^2\gamma_1^2 + a_2^2\gamma_2^2 \tag{A.41}$$

$$\Gamma_{12} = a_1 a_2\gamma_1\gamma_2\gamma_3 \tag{A.42}$$

$$\Gamma_{13} = \psi_{11}\psi_{21}\psi_{31} \tag{A.43}$$

$$\vartheta = \frac{\rho_f\omega^2}{(m\omega^2 - \mathrm{i}b\omega)} \tag{A.44}$$

$$h_i = \left(\frac{1}{\rho_f\omega^2} + a_i\right)\gamma_i\vartheta\ ,\ i = 1,2 \tag{A.45}$$

$$g_i = 2a_i\gamma_i\ ,\ i = 1,2 \tag{A.46}$$

$$g_3 = \lambda\chi_1 - 2\mu a_1\gamma_1^2 - \alpha \tag{A.47}$$

$$g_4 = \lambda\chi_2 - 2\mu a_2\gamma_2^2 - \alpha \tag{A.48}$$

Explicit expressions of the elements of $\mathbf{K}^{(N+1)}$ (Senjuntichai *et al.* 2019)

1st row:

$$\tilde{k}_{11} = \frac{\mu}{R_S}\left\{a_1\left[k_x^2\gamma_1 + \gamma_3(k_y^2 - \gamma_1\gamma_3)\right] - a_2\left[k_x^2\gamma_2 + \gamma_3(k_y^2 - \gamma_2\gamma_3)\right]\right\} \tag{B.1}$$

$$\tilde{k}_{12} = \frac{\mu k_x k_y}{R_S}\left[a_1(\gamma_1 - \gamma_3) - a_2(\gamma_2 - \gamma_3)\right] \tag{B.2}$$

$$\tilde{k}_{13} = \frac{\mu k_x}{R_S}\left[a_1(k^2 - 2\gamma_1\gamma_3 + \gamma_3^2) - a_2(k^2 - 2\gamma_2\gamma_3 + \gamma_3^2)\right] \tag{B.3}$$

$$\tilde{k}_{14} = -\frac{S^2\mu a_1 a_2 k_x(\gamma_1 - \gamma_2)}{R_S} \tag{B.4}$$

2nd row:

$$\tilde{k}_{22} = \frac{\mu}{R_S}\left\{a_1\left[k_y^2\gamma_1 + \gamma_3(k_x^2 - \gamma_1\gamma_3)\right] - a_2\left[k_y^2\gamma_2 + \gamma_3(k_x^2 - \gamma_2\gamma_3)\right]\right\} \tag{B.5}$$

$$\tilde{k}_{23} = \frac{\mu k_y}{R_S}\left[a_1(k^2 - 2\gamma_1\gamma_3 + \gamma_3^2) - a_2(k^2 - 2\gamma_2\gamma_3 + \gamma_3^2)\right] \tag{B.6}$$

$$\tilde{k}_{24} = -\frac{S^2\mu a_1 a_2 k_y(\gamma_1 - \gamma_2)}{R_S} \tag{B.7}$$

3rd row:

$$\tilde{k}_{33} = \frac{\mu\gamma_3}{R_S}\left[g_3 - g_4 + 2(a_1 - a_2)\,k^2\right] \tag{B.8}$$

$$\tilde{k}_{34} = \frac{\mu}{R_S}\left\{-a_1 g_4(k^2 - \gamma_1\gamma_3) + a_2\left[2a_1 k^2(\gamma_1 - \gamma_2)\gamma_3 + g_3(k^2 - \gamma_2\gamma_3)\right]\right\} \tag{B.9}$$

4th row:

$$\tilde{k}_{44} = \frac{a_1 h_2(k^2 - \gamma_1\gamma_3) - a_2\left[-\vartheta a_1 k^2(\gamma_1 - \gamma_2) + h_1(k_s - \gamma_2\gamma_3)\right]}{R_S} \tag{B.10}$$

where $R_S = a_1(k^2 - \gamma_1\gamma_3) - a_2(k^2 - \gamma_2\gamma_3)$ (B.11)